

# Internal reactions in the (Mg, Me)O system

D. L. RICOULT, H. SCHMALZRIED

*Institut für Physikalische Chemie, Callinstrasse 3-3A, D-3000 Hannover, Federal Republic of Germany*

Single- and polycrystals of (Mg, Me)O (Me = Fe, Co, Ni) have been oxidized or reduced under appropriate conditions of oxygen partial pressure, at temperatures ranging from 973 to 1673 K. The reaction always occurred internally and yielded a two-phase layer. The growth kinetics of this layer were measured and can be interpreted in terms of cation diffusion. The variability of the microstructures developed is emphasized and the effect of temperature, oxygen partial pressure and initial concentration in Me are discussed.

## 1. Introduction

The basic concepts of the internal oxidation of metal alloys have been drawn by Wagner [1], who has shown that the oxidation of a metal alloy (A, B), in which A is a more noble metal than B, may result in a dispersion of BO precipitates in the metal matrix impoverished in B. It has also been shown [2, 3] that the same morphology can occur upon further oxidation of a mixed oxide (A, B)O to higher oxidized forms like (A, B)<sub>3</sub>O<sub>4</sub> or (A, B)<sub>2</sub>O<sub>3</sub> (where A is the more noble metal), as well as upon reduction of these oxides to lower oxidation states of the B-cation, or even to metal (for the range of oxygen partial pressure considered here, A is assumed to remain ionized and to stay in the 2+ valence state). In this latter case, the final product is a dispersion of metal particles (B) in the oxide matrix which normally consists of almost pure AO. A detailed formal treatment of the kinetics of internal reactions in oxides is given in [2, 3]. A qualitative understanding of the phenomenon can be obtained by studying Fig. 1. In Fig. 1a, for example, an increase of oxygen activity is applied to the surface of the mixed oxide crystal (A, B)O. As a result, an internal oxidation front moves toward the inside of the material. At this reaction front ( $\xi''$ ), the precipitation of new spinel particles occurs, leading to the formation of a two-phase layer between the crystal surface and  $\xi''$ . The progression of the front ( $\xi''$ ) must be looked at as the macroscopic result of point-defect transport which conveys the higher oxygen chemical potential of the surface throughout the crystal. Thus, both the internal oxidation and the internal reduction can occur without any transport of oxygen in the crystal. In other words, the oxygen activity in the bulk of the crystal can equilibrate with that of the ambient atmosphere solely by diffusion of cationic and electronic defect species, whose concentrations, in local equilibrium, are correlated to the chemical potential of oxygen. For example, for the sake of charge compensation, electron holes (or electrons) must diffuse (or counterdiffuse) along with the cation vacancies. In fact, in the materials considered in this study, oxygen has always been experimentally identified as being the slowest bulk diffusing species (see, for example, [4]).

Here the oxygen sublattice will be considered as immobile. However, whereas internal oxidation and reduction involving oxides can easily be structurally visualized in terms of cation diffusion (if the oxide volume per mole of oxygen is approximately constant), whereby the oxygens are only locally rearranged to assume the structure of the product precipitates (from spinel structure to  $\alpha$ -corundum structure, for instance), the situation is far from being trivial in the case of reduction of the oxide to the metal phase. In this limiting case, the precipitation of the metal phase (B), out of a wüstite-type parent phase (A, B)O, for instance, requires that the oxygen sublattice locally "disappears" to leave room for the new metal particles. This problem will be addressed in greater detail in Section 3.

It is obvious that internal reactions will greatly affect material properties such as mechanical behaviour [5] and electrical conductivity [6]. In this respect, one of the decisive parameters will be the morphology of the precipitates. In this work it is intended to confront the previously proposed defect model with our experimental observations. We will emphasize the variability of the morphology developed and give new experimental observations which could help to understand the processes that may control it.

The systems investigated here are all of the type (Mg, Me)O, where Me is iron, nickel or cobalt. The oxidation and reduction experiments performed on these materials are indicated in the schematic phase diagram of Fig. 2, as arrows 1 and 2, respectively.

## 2. Experimental details

### 2.1. Internal oxidation

The first system selected for this study was a mixed oxide of magnesium and iron, (Mg, Fe)O. The oxidation of this material from the wüstite phase to the spinel + wüstite phase field was expected to be of particular interest for the following reasons: (i) the solubility of iron in MgO wüstite in equilibrium with MgFe<sub>2</sub>O<sub>4</sub> spinel becomes very small in air at temperatures lower than 1373 K [7] (the spinel phase can be somewhat non-stoichiometric, (Mg, Fe)<sub>3</sub>O<sub>4</sub>, but will be referred to as MgFe<sub>2</sub>O<sub>4</sub> in this paper), and (ii)

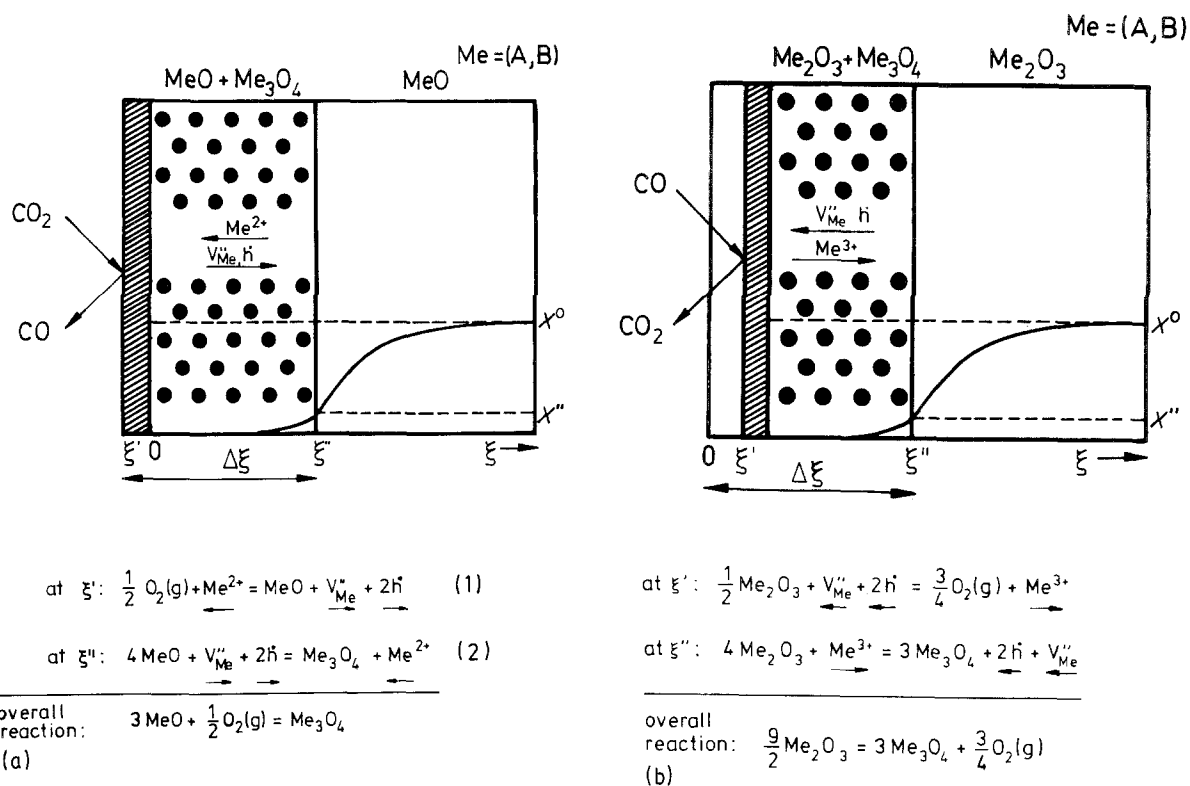


Figure 1 Point defect equations and schematic representation of (a) the internal oxidation of a mixed oxide (A, B)O, and (b) the internal reduction of a mixed oxide (A, B)<sub>2</sub>O<sub>3</sub>.

the precipitation of spinel MgFe<sub>2</sub>O<sub>4</sub> will lead to a depletion of the wüstite matrix in iron, rendering it very sluggish for all further diffusion-controlled processes (because the concentration of defects available for diffusion is related to the iron content by point defect thermodynamics). The role of dislocations or of subgrain boundaries is then expected to become dominant in the kinetics of further oxidation of the crystal. This effect is less marked in systems like (Ni, Fe)O or (Fe, Ti)O where the cation diffusion in the NiO or FeO crystalline matrix after internal oxidation is still appreciable.

Two types of material have been used for this study. Firstly, single crystals of (Mg, Fe)O with 1% (cation per cent) iron were bought from Spicer Ltd, UK. The green colour of the transparent crystals strongly

suggests that iron is in its divalent state. Secondly, polycrystals were prepared by us by various methods. The highest density was obtained for hot-pressed pellets prepared from gel coprecipitation of nitrate solutions of magnesium and iron. The hot-pressing was carried out at 1573 K in an aluminium oxide die (built in our laboratory) through which a constant flow of CO/CO<sub>2</sub> = 0.01 was maintained to prevent a premature oxidation of the sample. It should be noted that the widely used graphite dies were inadequate for our purpose, as they would reduce the sample, leading to precipitation of metallic iron. These materials were then cleaved on the {001} faces (single crystals) or sawn (polycrystals) into parallelepipeds of average size 2 × 2 × 3 mm<sup>3</sup>. In order to investigate a possible effect of the surface finish on the oxidation kinetics, we

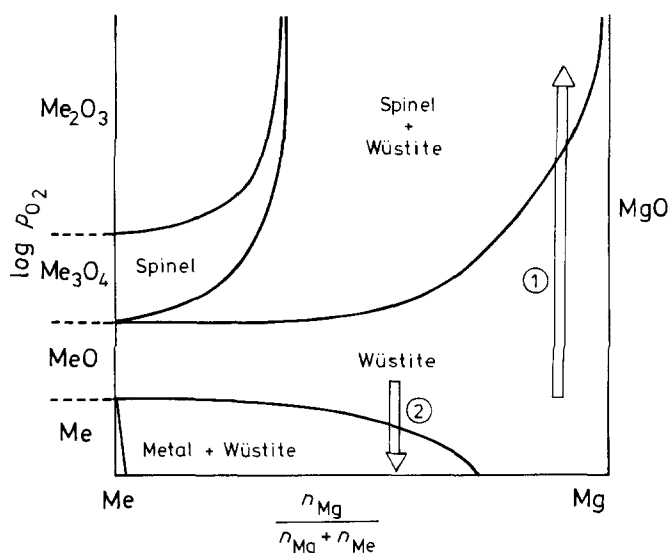


Figure 2 Schematic phase diagram of the second kind for the MeO-MgO system, where Me is Fe, Co or Ni.

used several methods to prepare the single crystals. Some of them were not further prepared after cleavage; broad cleavage steps were visible on the {001} faces. Others were mechanically polished with 1  $\mu\text{m}$  diamond powder. Finally, a few of these specimens were chemically polished by short immersion in boiling phosphoric acid.

The single crystalline samples underwent various heat treatments prior to their oxidation. A first batch was equilibrated for 72 h at 1673 K in air. A second batch was also maintained at 1673 K for 72 h, but in a reducing atmosphere of  $\text{CO}/\text{CO}_2 = 0.35$  ( $p_{\text{O}_2} \approx 10^{-9}$  MPa). Finally, as-received crystals were directly oxidized. Based on technical information provided to us by the crystal grower, it is reasonable to assume that the defect structure of these crystals is in equilibrium with air at temperatures higher than 2300 K. In all three cases the crystals were still green before the oxidation heat-treatment, hinting that no precipitation of spinel had unexpectedly started. The oxidation experiments were subsequently carried out at lower temperatures between 973 and 1373 K, in air. After oxidation, the samples were embedded in epoxy, sawn into two halves, and polished to enable observation with either an optical microscope, or a scanning electron microscope.

## 2.2. Internal reduction

The internal reduction experiments were carried out on single-crystalline materials of various types: (Mg, Fe)O single-crystals bought from Spicer Ltd, UK, analogous to those used for the oxidation experiments, (Mg, Ni)O and (Mg, Co)O single-crystals prepared in our laboratory by interdiffusion between the appropriate powders and commercial MgO single-crystals. For this purpose, MgO single-crystals were cleaved in parallelepipeds whose smallest dimension rarely exceeded 1.5 mm. Several of these samples were packed either in CoO or (Mg, Co)O powder, or in (Mg, Ni)O powder inside a prereacted alumina crucible, which itself was hung with Pt–Rh wire in the hot zone of either a Tamann furnace heated at 1973 K, or of a silicium carbide furnace at 1633 K. The final composition of the crystals depended upon the duration of this anneal, but also upon the sample geometry and the cation ratio of the (Mg, Me)O-package powder used. The interdiffusion anneal was followed by an homogenization run performed at 1973 K for about 3 days. The samples were then rapidly pulled out of the furnace. As an example, after interdiffusion with NiO powder at 1633 K for 650 h and homogenization for 72 h at 1873 K, a 0.8 mm thick MgO crystal was analysed to contain 20 cation percent Ni. It should, however, be noticed that the homogenization of similarly treated crystals often lacked reproducibility, yielding homogeneous crystals as well as crystals with a steep nickel or cobalt concentration gradient at their surface. If it is assumed that most of the transport between powder and crystal takes place via the gas phase, one concludes that the compaction does not always lead to an homogeneous activity of the gas phase around the samples. The reduction experiments were performed in graphite

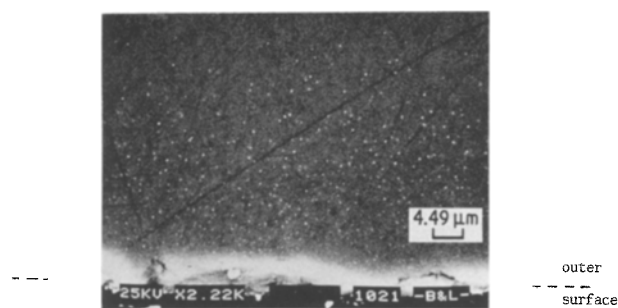


Figure 3 Scanning electron micrograph of a reaction layer in a  $(\text{Mg}_{0.99}\text{Fe}_{0.01})\text{O}$  single-crystal oxidized in air at 1173 K for 10 h. The spinel precipitates appear as white dots (back-scattered electron mode).

ampoules at temperatures ranging from 1273 to 1673 K. In these conditions, the very low partial pressure of oxygen at the sample surface should be approximately fixed by the C/CO buffer. The samples were prepared for microscopic observation in the same way as described for the oxidized samples.

## 3. Results and discussion

### 3.1. Internal oxidation

A typical microstructure resulting from an oxidation experiment is presented in Fig. 3, as recorded with a scanning microscope. Whereas precipitates in the micrometer range occur upon oxidation of both the as-received crystals and those preannealed in  $\text{CO}/\text{CO}_2$  at 1673 K, no second-phase particles could be detected in the crystals preannealed in air at 1673 K, although all three types of sample were brownish-red after oxidation. The micrometre-size precipitates observed with the scanning microscope in the oxidized as-received samples occurred in a well-defined temperature–time domain, as shown in Fig. 4. It should be noted that even though we did not identify precipitates in all crystals oxidized at 1273 and 1323 K, the initial green colour of these crystals also turned to brown after oxidation. This colour change could be associated with spinel precipitates of smaller size, below the resolution of our microscope.

The observed precipitates were found in a reaction layer which grows towards the inside of the crystal roughly as the square root of time, see Fig. 5. However, for larger values of the reaction layer thickness,

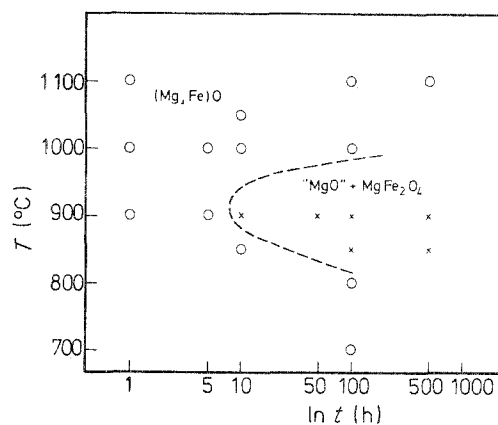


Figure 4 Temperature–time–formation diagram. Domain of observation of the spinel precipitates in oxidized  $(\text{Mg}_{0.99}\text{Fe}_{0.01})\text{O}$ .

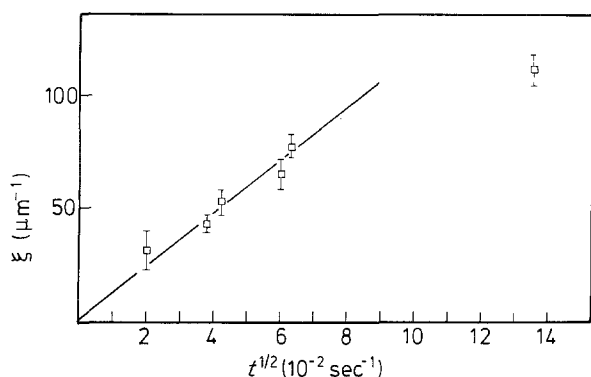


Figure 5 Oxidation layer thickness ( $\xi$ ) plotted against time for the oxidation of ( $\square$ ) ( $\text{Mg}_{0.99}\text{Fe}_{0.01}$ )O single crystals.  $T = 900^\circ\text{C}$ .

$\xi$ , the parabolic dependence does not hold. As the reaction proceeds, two opposing factors grow in importance: (i) the surface area of the reaction front decreases as it moves deeper into the crystal, and (ii) the depletion in iron of the matrix between the precipitates, behind the reaction front, slows down more and more the diffusion of the cations as indicated in Fig. 1a. According to Fig. 5, the second factor has a dominant effect. If in the early stages of the reaction the layer is assumed to grow as  $\Delta\xi^2 = 2k_p t$  (where  $k_p$  is the parabolic rate constant, see [8]), we find that  $k_p \approx 5 \times 10^{-11} \text{ cm}^2 \text{ sec}^{-1}$  at 1173 K. From theory,  $k_p$  can be approximated to the cation diffusion in the matrix:  $k_p \approx 2zD_{\text{Mg}}/x_{\text{Me}}^0$ , with  $z$  being a numerical factor of the order of one, reflecting the diffusion enhancement due to the compensating electronic carriers present in oxide semiconductors,  $D_{\text{Mg}}$  being the magnesium self-diffusion coefficient, and  $x_{\text{Me}}^0$  the concentration in Me (= Fe) of the unreacted matrix. The value estimated here for  $k_p$  is in good agreement with the theory and with the data available in the literature [9] for the self-diffusion coefficient of magnesium,  $D_{\text{Mg}}$ , in MgO. The diverse preparations of the sample surface appear to have no effect on the oxidation kinetics.

It should be emphasized that an exact measurement of the oxidation layer thickness is often difficult, because of the presence of isolated dislocations or of subgrain boundaries which are preferentially decorated by spinel particles, as they constitute sites for

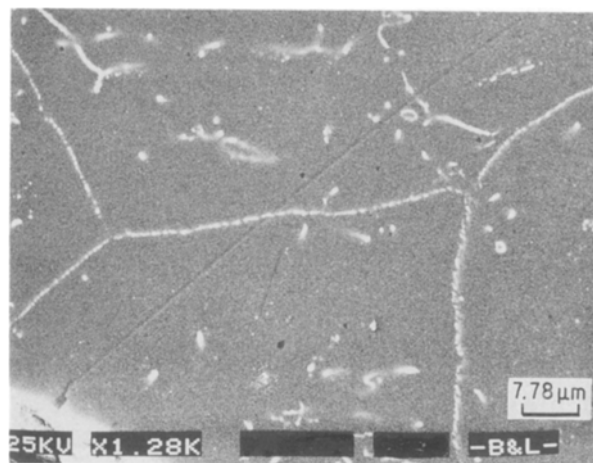


Figure 6 Scanning electron micrograph of preferential precipitation of spinel at subgrain boundaries present in a single crystal of ( $\text{Mg}_{0.99}\text{Fe}_{0.01}$ )O.

heterogeneous nucleation as well as short circuit paths for diffusion. Such an example of preferential spinel precipitation may be seen in Fig. 6. Because of this effect, we have restricted our reaction layer thickness measurements to areas of free dislocations. The morphology of the precipitates, especially when they occur in the defect-free bulk, often exhibits a strong influence on the crystal structure of the materials. The projected shape of the precipitates, as it appears in the recorded micrographs, is a rhombus or a cross. In the latter case, a partial constriction of the arms of the cross, close to its centre, is sometimes observed (Fig. 7a), which could correspond to an early stage of dendritic morphology. The main directions of the crosses are parallel to the  $\langle 100 \rangle$  directions of the host crystal. This morphology is very similar to that observed for  $\text{NiFe}_2\text{O}_4$  precipitates in a matrix of NiO, after internal oxidation [10]. It reflects the minimum elastic modulus in the  $\langle 100 \rangle$  directions of the rock-salt structure. The rhombic precipitates are oriented so that the corners of the rhombus point towards the  $\langle 110 \rangle$  directions of the matrix. This morphology could either be an early stage of the cross morphology or the result of cross-sectioning the arms of the crosses for the smallest rhombus. In many instances, the recorded image of the precipitates reveals a diagonal

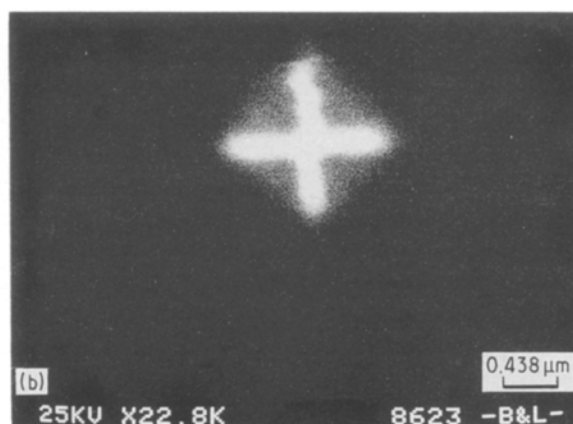
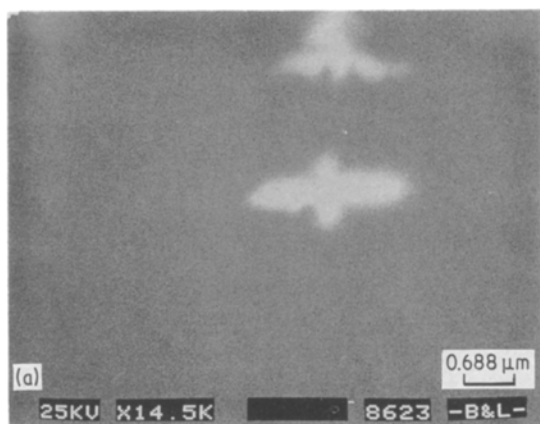


Figure 7 (a) and (b) Back-scattered electron images showing the morphology of spinel precipitates in an oxidized single crystal of ( $\text{Mg}_{0.99}\text{Fe}_{0.01}$ )O.

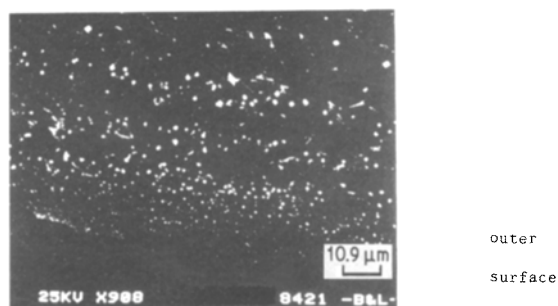


Figure 8 Precipitation bands of spinel during internal oxidation of a  $(\text{Mg}_{0.99}, \text{Fe}_{0.01})\text{O}$  single crystal at 1173 K for 500 h.

cross centred inside a square (Fig. 7b). The three-dimensional shape of the precipitate could then be the intersection of three orthogonal plates lying in the  $\{001\}$  planes, corresponding to the growth anisotropy. In all cases, the largest precipitates observed were  $2\ \mu\text{m}$  in size.

In general, the size of the precipitates increased from the outer surface toward the crystal centre, whereas their number decreased, reflecting a slowing down of the nucleation rate as the reaction proceeds. In a few cases, the precipitates have formed periodically (Fig. 8) in much the same way as the periodic precipitation named after Liesegang [11]. The periodicity of the precipitation would be the result of the concurrent diffusion processes depicted in Fig. 1a, and of the slow build-up of the “supersaturation” needed for the precipitates to form. A qualitative model is presented in an earlier work [12]. The phenomenon is expected to occur and is actually found under very restricted conditions of iron concentration, concentration of preformed nucleation sites (e.g. dislocations) and temperature.

The observation that no precipitates could be detected in samples preannealed in air at 1673 K can be tentatively explained in the following way: under these annealing conditions, the  $\text{Fe}^{3+}/(\text{Fe}^{2+} + \text{Fe}^{3+})$  ratio is likely to be high, in agreement with the measurements of Brynestad and Flood [13]. In other words, the  $\text{Fe}^{3+}$  ions necessary to be incorporated into the spinel structure upon oxidation at lower temperature are already present before the reaction anneal, diluted in the wüstite phase. As the oxidation anneal at 1173 K proceeds, a massive homogeneous nucleation of spinel occurs as a response to the cooling, followed by a growth episode yielding homogeneously dispersed second-phase spinel particles which are so small that they are not detectable with our scanning electron microscope [14]. This precipitation phenomenon, resulting mostly from the temperature decrease, is quite different from the progressive isothermal internal oxidation observed in either the “as-received” samples (equilibrated at very high temperature, i.e. most of the iron is in a ferrous state) or in those annealed at 1673 K in reducing conditions (also high ferrous iron content). Only then are the kinetics of this isothermal reaction dictated by the defect fluxes, driven by the gradient of oxygen chemical potential, existing between the crystal surface and its bulk.

In polycrystals, if the grain size is small and if the

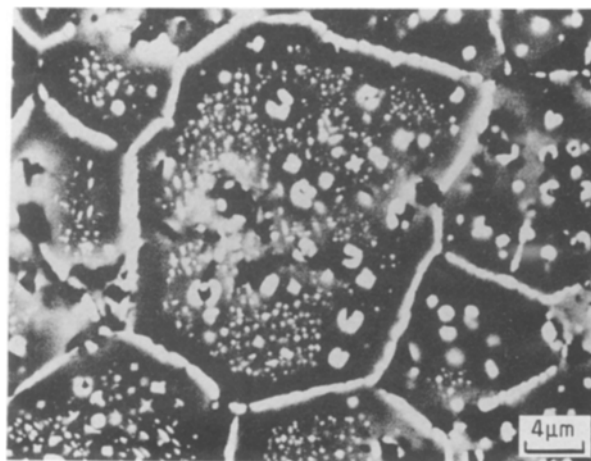


Figure 9 Scanning electron micrograph of an oxidized  $(\text{Mg}_{0.9}\text{Fe}_{0.1})\text{O}$  polycrystal (oxidation in air, at 1273 K for 100 h).

diffusivity along the grain boundaries is high, it is not possible to measure the kinetics of the bulk reaction: the grain boundaries are first preferentially decorated, and the small grains are afterwards very quickly reacted through. In addition, as a consequence of the preferential decoration of the boundaries, a depletion of the iron in the matrix is observed at the periphery of the grains (Fig. 9). The breadth of the depleted zone is about  $2\ \mu\text{m}$ . At iron concentrations of  $n_{\text{Fe}}/n_{\text{Mg}} + n_{\text{Fe}} = 0.10$ , the precipitate morphology in the reduced polycrystals appears to be more diverse than in the previously described single-crystals and their size often exceeds  $2\ \mu\text{m}$ . However, the interaction of the crystal structures of the two phases is still strong and affects the precipitate morphology: numerous cross-shaped precipitates can be seen (Figs 9 and 10).

The structural nature of the precipitates was ascertained by crushing a few oxidized polycrystals and analysing them in an X-ray diffractometer. The intensity peaks were unequivocally identified as being the characteristic reflections of MgO and  $\text{MgFe}_2\text{O}_4$  spinel.

### 3.2. Internal reduction

There is no basic conceptual difficulty to understand internal oxidation processes. This is not so for internal reduction processes when, for instance, metal is locally

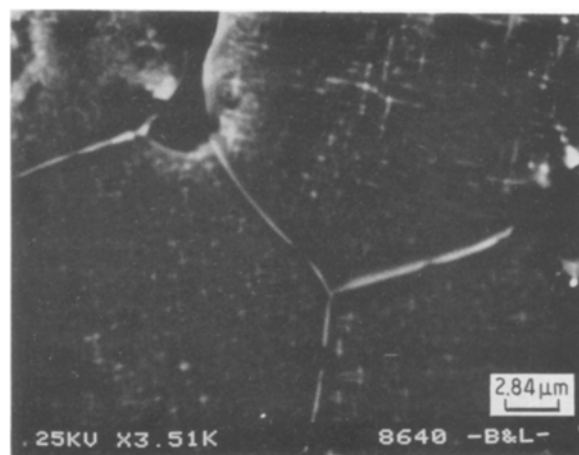


Figure 10 Cross-shaped spinel precipitates evolved during internal oxidation of polycrystalline  $(\text{Mg}_{0.9}\text{Fe}_{0.1})\text{O}$  (back-scattered electron mode).

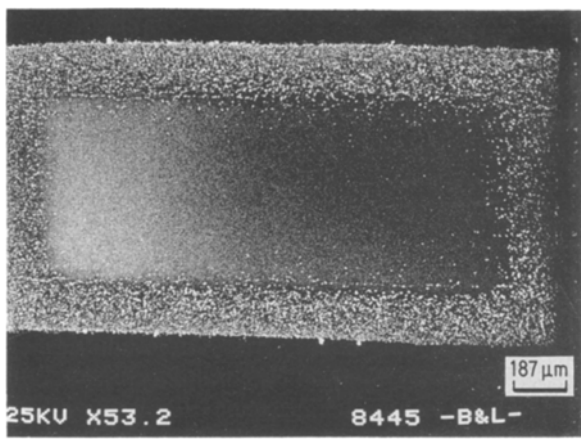


Figure 11 Internal reduction of a  $(\text{Mg}_{0.91}\text{Co}_{0.09})\text{O}$  single crystal at 1673 K for 12 h (secondary electron image).

precipitated inside the oxide matrix at the reaction front. In this case, the question which arises, assuming that the oxygen sublattice is immobile, is: how and where to provide room for the metal precipitates in the oxide matrix? This obviously cannot be done by diffusing only metal into the matrix, i.e. by diffusing cation vacancies formed at the precipitate surface to the outer surface of the crystal, as this diffusion would result in an increase of the local volume. Rather, oxygen has to be removed. Oxygen lattice diffusion being too slow to account for this removal, other mechanisms must be present. Several possibilities exist for outward oxygen diffusion: (i) along a continuous precipitate, which would grow as a spike or, after branching, tree-like from the crystal outer surface. The diffusion can then take place either through the bulk metal or along the oxide-metal interface. Because of the smaller molar volume of the metal phase relative to that of the oxide matrix, pores can exist along this interface; (ii) along lattice faults formed during the metal precipitation process (dislocations, small-angle boundaries) which could act as short-circuit diffusion paths between otherwise isolated precipitates. This process would become relevant if the oxygen diffusivity along the dislocation pipes would match the cation diffusivity through the oxide bulk; (iii) along cracks which could form because of the local volume increase referred to above. The possibility for these processes to occur will be discussed

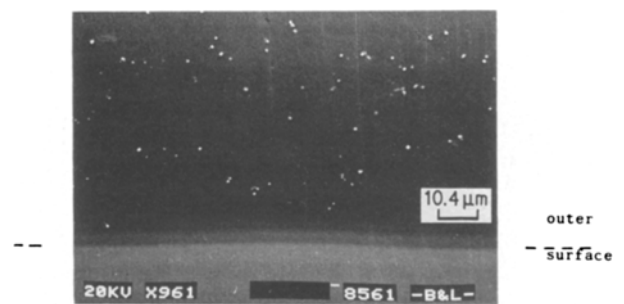


Figure 12 Internal reduction of a  $(\text{Mg}_{0.99}\text{Fe}_{0.01})\text{O}$  single crystal at 1673 K for 18 h (secondary electron image).

in connection with the presentation of our experimental results.

Regardless of the previous comments, internal reduction does occur. A typical product of internal reduction may be seen in Fig. 11 for a single-crystal of  $(\text{Mg}, \text{Co})\text{O}$ . The reaction layer is composed of metal precipitates in a depleted oxide matrix. Its thickness is remarkably constant all around the specimen. The reaction front is straight and shows little or no rounding at the corners, even at this relatively advanced stage of the reaction. For better comparison with the structure evolved during internal oxidation, a single-crystal of  $(\text{Mg}_{0.99}\text{Fe}_{0.01})\text{O}$  was reduced at 1673 K for 18 h. For this low concentration, the reaction layer shown in Fig. 12 is not as clear cut. This figure should be compared with Fig. 3. Although they have a size similar to that of the spinel precipitates, the visible metal particles are much less numerous than the spinel precipitates, a likely consequence of the difference in molar volume per iron atom between the two phases. This observation is somewhat surprising as it implies that iron must diffuse over relatively large distances from the matrix (which thereby becomes more and more sluggish for diffusion) to the precipitates. The spatial distribution of the metal particles appears to be close to random and no size trend is to be found. The morphology of the precipitates is more uniform than it was in the oxidized crystals: in the micrographs, the projection of most metal precipitates is a rhombus (Fig. 13), regardless of the precipitate size. Occasional observations of streaks of back-scattered intensity, as in Fig. 13b, suggest that at least some of the precipitates are actually flat and plate-like.

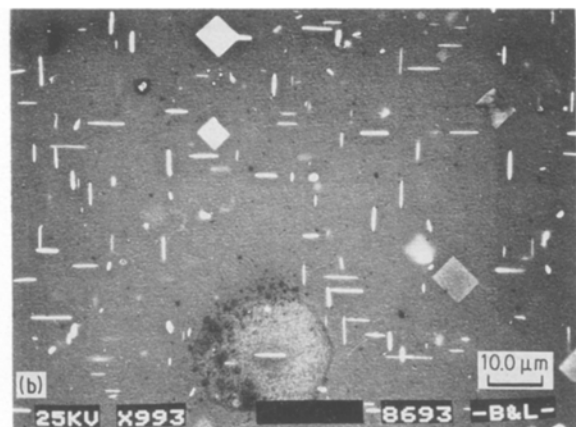
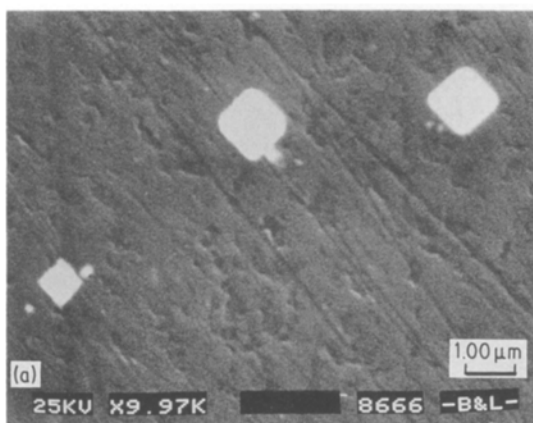


Figure 13 (a) and (b) Scanning electron micrograph showing the morphology of iron precipitates in a reduced  $(\text{Mg}_{0.99}\text{Fe}_{0.01})\text{O}$  single crystal.

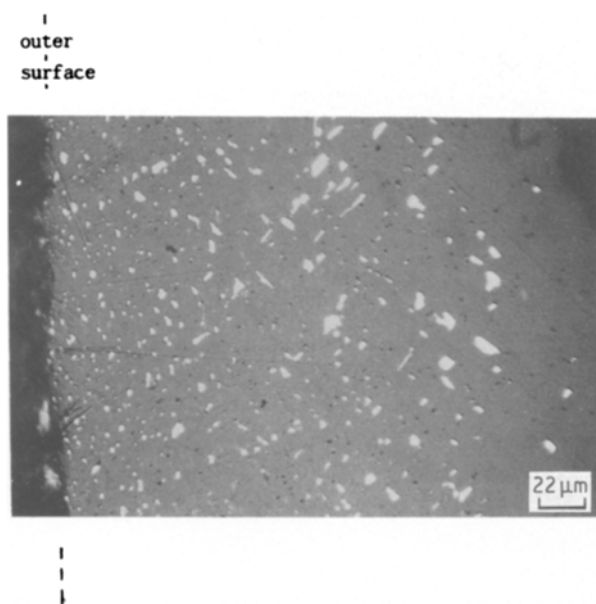


Figure 14 Optical micrograph of the reaction layer in a  $(\text{Mg}_{0.9}\text{Co}_{0.1})\text{O}$  single crystal reduced at 1673 K for 12 h.

Although octahedron-shaped particles would be favoured from an argument based on surface energy considerations, Nabarro [15] has shown that plate-shaped or disc-shaped precipitate morphologies are preferred above a certain size corresponding to the loss of coherency between particle- and host-lattices, and originate because the growth then takes place only along the elastically soft directions of the host crystal, namely along the  $\langle 001 \rangle$  and  $\langle 101 \rangle$  directions in the material studied here. Indeed, the corners of the rhombus-shaped particles always point in the  $\langle 001 \rangle$  directions of the oxide matrix and the faces of the rhombi are  $\{101\}$  surfaces. The streaks observed in the micrographs are always parallel to the  $\langle 001 \rangle$  directions. The largest precipitates observed were  $3 \mu\text{m}$ . (Similarly, plate-shaped particles of  $\text{NiCr}_2\text{O}_4$  spinel were found in oxidized crystals of the  $\text{NiO}-\text{Cr}_2\text{O}_3$  system [16].)

As the concentration of the reducible metal (more noble metal) is increased, the precipitate size increases as well. In Fig. 14, the precipitates of cobalt formed by the reduction of a  $(\text{Mg}_{0.91}\text{Co}_{0.09})\text{O}$  single-crystal

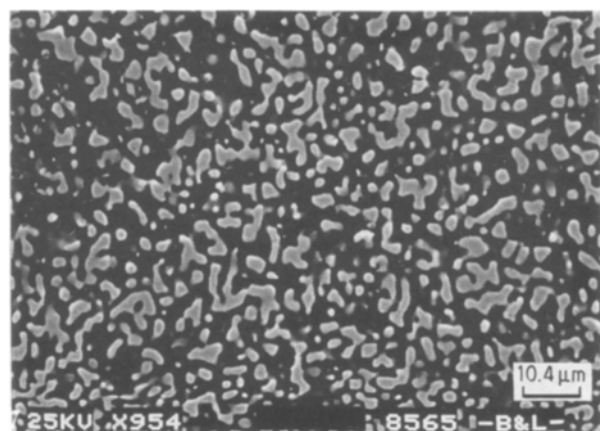


Figure 15 Morphology of the nickel precipitates formed during internal reduction of a  $(\text{Mg}_{0.8}\text{Ni}_{0.2})\text{O}$  single crystal at 1673 K.

outer  
surface

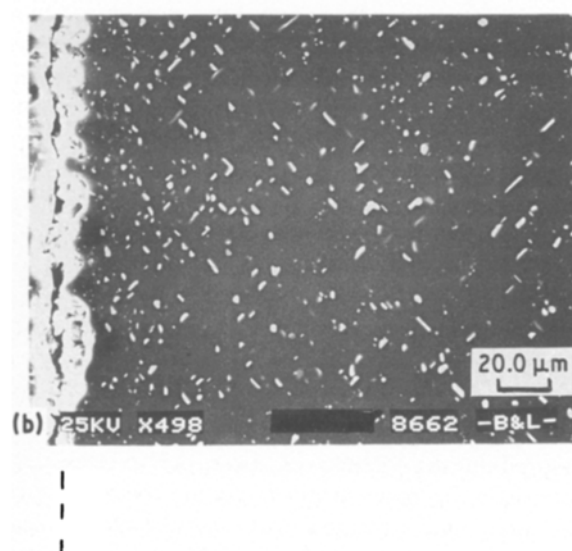
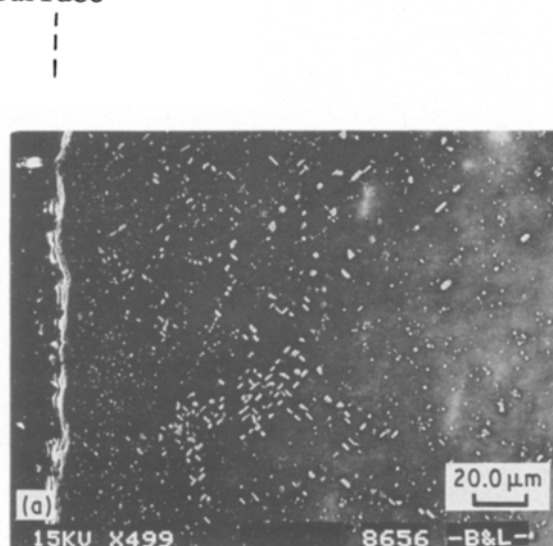


Figure 16 Internal reduction of a  $(\text{Mg}_{0.91}\text{Co}_{0.09})\text{O}$  single crystal at 1673 K: (a) after 5 h and (b) after 29 h.

become larger as they are deeper located, probably due to the slowing down of the supersaturation build-up and therefore of the nucleation rate [12]. They adopt a plate-like shape elongated along the  $\langle 101 \rangle$  directions of the matrix. At still higher concentrations of the minority cation species, the precipitates coalesce and take an amoeba-like morphology. This is the case in Fig. 15 for a reduced  $(\text{Mg}_{0.80}\text{Ni}_{0.20})\text{O}$  single-crystal. The general tendency for the precipitate size to increase from the outer surface toward the bulk of the material (also observed for internal oxidation) vanishes after extended anneals following completion of the reduction reaction. In Fig. 16a, the reaction layer has just reached the centre of a  $(\text{Mg}_{0.91}\text{Co}_{0.09})\text{O}$  single-crystal. After an annealing of 48 h at the same temperature, 1673 K, most of the small precipitates have disappeared to the benefit of the larger ones which grew still larger, Fig. 16b. This observation indicates that Ostwald ripening takes place in these materials. In the oxide shown in Fig. 16, the depletion in cobalt in the matrix between the metal precipitates is not

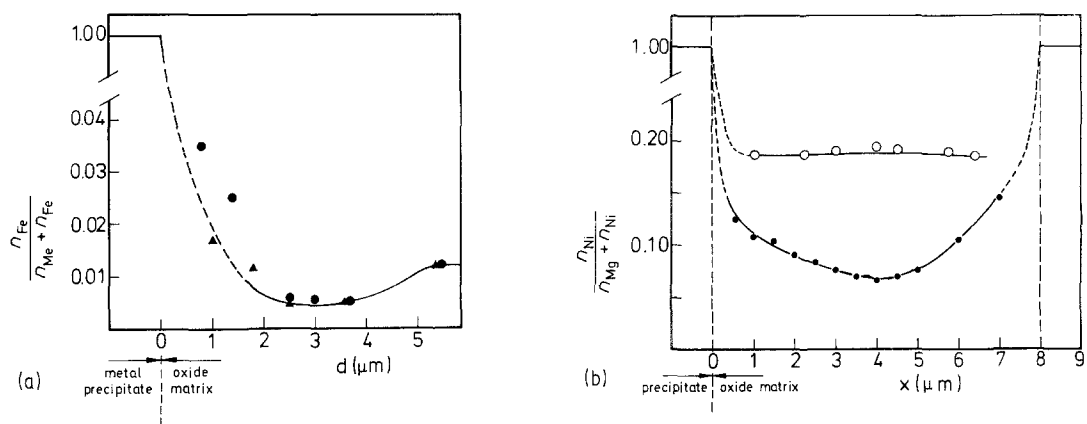


Figure 17 Energy dispersive analyses of (a) the iron concentration in the oxide matrix surrounding a metal precipitate (the triangles and dots correspond to different measurements), and (b) the nickel concentration in the oxide matrix between two metal precipitates (solid dots) and ahead of the foremost precipitate of the reaction layer (open circles).

complete (about 1.5 cation per cent Co remains in solution) which would kinetically allow for the necessary long-range transport from one small precipitate to a large one. For this reason, this phenomenon is unlikely to occur for low concentrations of the minority cation.

Upon precipitation of the metal phase, the matrix is depleted of the corresponding element. This depletion has been measured by energy dispersive analysis as being a shell of low Me-concentration around each Me-precipitate. A typical analysis is reported in Fig. 17a for the region surrounding a metallic precipitate in  $(\text{Mg}_{0.99}\text{Fe}_{0.01})\text{O}$ . The depleted shell is about  $5\ \mu\text{m}$  wide. A similar analysis conducted in  $(\text{Mg}, \text{Ni})\text{O}$  for nickel precipitates at the reaction front, shows a different result (Fig. 17b): no depletion from the unreacted oxide matrix ahead of the reaction front was measured in the vicinity of these precipitates. For comparison, a concentration profile between two nickel precipitates located in the middle of the reaction layer is also shown in Fig. 17b. The gradient in the unreacted matrix ahead of the reaction front is small because the nickel concentration in the matrix is large. Moreover, because of this high nickel content, diffusion of nickel from the crystal interior to the reaction front is relatively fast and balances the nickel depletion taking place in the vicinity of the precipitates. In contrast, the oxide matrix within the reaction

layer contains less nickel, the concentration of which will decrease as the precipitates grow, until it has reached the equilibrium value given by the thermodynamics of the system.

If we plot the experimentally measured reduction layer thicknesses for the various  $(\text{Mg}, \text{Me})\text{O}$  single crystals, an approximate value of the corresponding reaction rate constant can be determined for the starting period of the internal reduction. This is done in Fig. 18. Although the dependence of the self-diffusion coefficients on the cation concentrations is not very well known in these mixed oxides, the values obtained for  $k_p$  here agree better with the estimated cation self-diffusion coefficients than with the bulk self-diffusion coefficients for oxygen. Schnehage *et al.* [17] measured the tracer diffusion coefficients for magnesium and cobalt in  $(\text{Co}_x\text{Mg}_{1-x})\text{O}$  mixed oxides. The extrapolation of their data to 1673 K,  $x = 0.1$  and  $p_{\text{O}_2} = 10^{-11}$  MPa yields  $D_{\text{Mg}}^* \approx 10^{-12}$   $\text{cm}^2 \text{sec}^{-1}$  and  $D_{\text{Co}}^* \approx 2 \times 10^{-11}$   $\text{cm}^2 \text{sec}^{-1}$ . No measurements of  $D_{\text{O}}^*$  are available for such mixed oxides. However, oxygen is known to diffuse orders of magnitude slower in the bulk of  $\text{MgO}$ , and it is very likely to behave in the same manner in the materials considered here. The approximate agreement of  $k_p$  and the derived  $D_{\text{cation}}$  in  $\text{MgO}$ , however, does not necessarily mean that the reduction process is controlled by cation diffusion. As discussed above, if oxygen diffuses out of the crystal along dislocation pipes, for example, the kinetics measured in Fig. 18 could be representative of this mechanism. In other words, internal reduction could then be rate-controlled by oxygen pipe diffusion rather than by cation bulk diffusion.

For the higher Me concentrations, the morphology of the precipitates should be considered with the greatest attention, because they can coalesce and form continuous paths to the outer surface, which affect the reduction mechanism. This possibility is strongly supported by Fig. 15, for example. Oxygen could then diffuse either along the interphase boundaries between matrix and metal precipitate, or through the metal phase itself. Here oxygen can diffuse orders of magnitude faster than in the oxides investigated. When such continuous short circuits for diffusion are not available, i.e. at lower Me-concentration, and when the

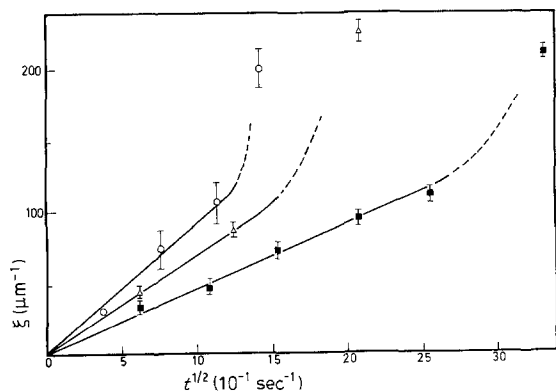


Figure 18 Kinetics of internal reduction at 1673 K of various  $(\text{Mg}, \text{Me})\text{O}$  single-crystals.  $T = 1400^\circ\text{C}$ ,  $(\blacksquare)$   $(\text{Mg}_{0.99}\text{Fe}_{0.01})\text{O}$ ,  $k_p = 1 \times 10^{-9}$   $\text{cm}^2 \text{sec}^{-1}$ ;  $(\triangle)$   $(\text{Mg}_{0.91}\text{Co}_{0.09})\text{O}$ ,  $k_p = 2 \times 10^{-9}$   $\text{cm}^2 \text{sec}^{-1}$ ;  $(\circ)$   $(\text{Mg}_{0.81}\text{Ni}_{0.19})\text{O}$ ,  $k_p = 4 \times 10^{-9}$   $\text{cm}^2 \text{sec}^{-1}$ .

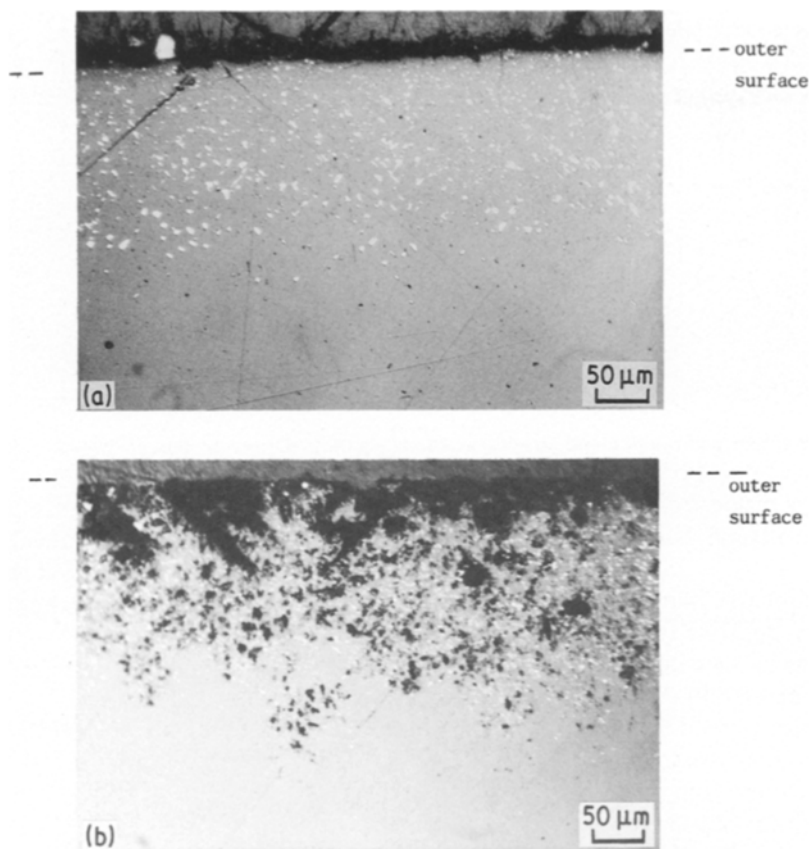


Figure 19 Internal reduction of a  $(\text{Mg}_{0.91}\text{Co}_{0.09})\text{O}$  single crystal (a) at 1673 K for 12 h, and (b) at 1283 K for 42.5 h.

kinetics for diffusion through the depleted oxide matrix are too slow, i.e. at low temperature, then internal reduction may have dramatic effects on the final microstructure. This statement is emphasized in Fig. 19. In Fig. 19a, a single crystal of  $(\text{Mg}_{0.91}\text{Co}_{0.09})\text{O}$  has been reduced at 1673 K. The precipitates have formed in the way described above and determine a very clearly confined two-phase reaction layer in which the depleted matrix is structurally undisturbed, at least at this scale. The depletion of the matrix in the reaction layer is such that the cation concentration half-way between two precipitates drops to or below 0.01. A crystal of exactly the same composition was reduced for the same duration at 1283 K. The reaction layer which grows during this experiment is shown in Fig. 19b. Although the advancement of the reaction front is comparable too, if not larger than, that measured in the experiment performed at 1673 K, the oxide lattice between the metal particles is now extremely porous. At the same time, the outer surface of the crystal is very rugged. This interface instability could result from the preferential outward diffusion of vacancies to imperfections of the outer surface (polishing scratches, cleavage steps, etc.), in much the same way as Yurek and Schmalzried [18] interpreted the porosity developing in a CoO single-crystal placed in a gradient of oxygen partial pressure. To understand the observation presented in Fig. 19, one should refer once again to Fig. 1b. In order for internal reduction to take place, metal cations must diffuse toward the reaction front and cation vacancies of the bulk (and electron holes) must be eliminated to the outer surface. In addition, oxygen must also diffuse out. At 1673 K, this elimination can take place by volume- or (dislocation) pipe diffusion. At 1283 K,

however, if the corresponding activation energy is too large, another mechanism takes over. As suggested by Fig. 19b, this mechanism could be diffusion through pores forming continuous channels to the outer surface.

### 3.3. Observations by transmission electron microscopy

Finally, it is appropriate to discuss the questions raised in the introduction: how does the oxygen lattice locally provide space for the newly-forming metal phase, i.e. how is the oxygen transported out of the crystal? A few reacted samples were thinned by argon bombardment and observed by transmission electron microscopy. The first sample shown in Fig. 20a is an oxidized polycrystal of composition  $(\text{Mg}_{0.9}\text{Fe}_{0.1})\text{O}$ . The influence of the crystal structure of the two phases on the shape of the spinel precipitate matrix is again obvious. The point which we wish to emphasize is the absence of dislocations in this sample (note, however, that dislocations have been observed around spinel precipitates in internally oxidized  $(\text{Ni}, \text{Fe})\text{O}$  [10]). The second sample investigated (Fig. 20b) is a single crystal of  $(\text{Mg}_{0.9}\text{Ni}_{0.1})\text{O}$  having undergone an internal reduction at 1673 K. Apart from the morphology of the nickel precipitates, the most striking feature is the high dislocation density in the vicinity of the metal particles. These dislocations, which locally organize themselves in low-angle boundaries, can certainly be ascribed to the positive reaction volume of the metal precipitates. Furthermore, they could very well provide a plausible diffusion path required for the oxygen ions to reach the outer surface, in order to make room for the newly formed metal precipitates. It

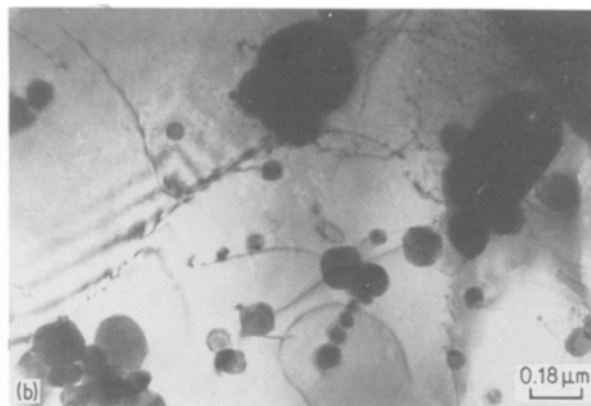
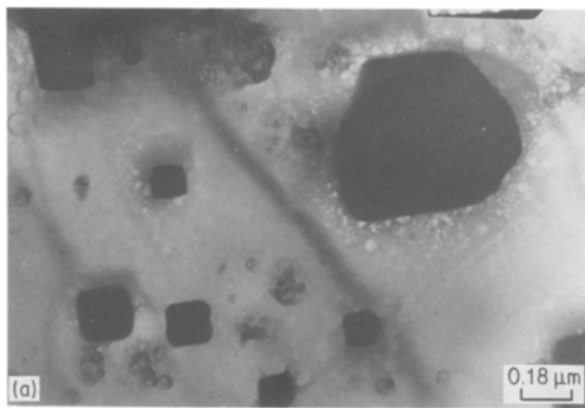


Figure 20 Transmission electron micrographs (bright field, two-beam condition) of (a) oxidized  $(\text{Mg}_{0.9}\text{Fe}_{0.1})\text{O}$ , and (b) reduced  $(\text{Mg}_{0.9}\text{Ni}_{0.1})\text{O}$ .

is well known that oxygen diffusion along dislocations can be much faster than through the crystal bulk [19, 20].

In the present investigation, no attempt was made to identify the atomistic mechanisms responsible for the formation of the initial metal nucleus in the oxide matrix. For example, the strain field generated in the matrix by the growth of a metal precipitate could be partly relaxed by local volume diffusion of oxygen from the site of the precipitate to dislocations present in the vicinity. Interactions of these dislocations into loops surrounding the growing particles would reduce the necessary bending of the lattice planes around the precipitates. More high-resolution transmission electron microscopy must be done on internally reduced samples in order to unravel this problem.

#### 4. Conclusions

New experimental observations of internal reactions occurring in mixed oxides of the  $(\text{Mg}, \text{Me})\text{O}$  system are reported. Both internal oxidation and internal reduction seem to be adequately described by the point defect model put forward earlier [2, 3]. In particular, the assumption that lattice oxygen plays a passive role in the transport processes proceeding during the reactions is justified, even for the precipitation of metal by reduction. Nevertheless, in this case, oxygen must be transported out of the crystal, which can for example be done via pipe diffusion along dislocations. The dislocations are likely generated under the influence of the high stresses associated with the growth of the metal particles. We have also shown that the morphology of the precipitation is very sensitive to the concentration of the minority cation, the temperature and the partial pressure of oxygen. Finally, we have presented experimental evidence that Ostwald ripening of the precipitates formed by internal reactions does occur.

#### Acknowledgements

The authors wish to thank K. Majoni for the invaluable technical assistance she provided throughout this work. The financial support of the Volkswagen Foundation is gratefully acknowledged.

#### References

1. C. WAGNER, *Ber. Bunsenges. Phys. Chem.* **63** (1959) 772.
2. H. SCHMALZRIED, *ibid.* **87** (1983) 551.
3. *Idem. ibid.* **89** (1984) 124.
4. R. FREER, *J. Mater. Sci.* **15** (1980) 803.
5. B. REPPICH and H. KNOCH, in "Deformation of ceramic materials", edited by R. C. Bradt and R. E. Tressler (Plenum, New York, 1983) p. 243.
6. V. B. TARE and J. B. WAGNER, *J. Appl. Phys.* **54** (1983) 252.
7. D. R. SEMPOLENSKI and W. D. KINGERY, *J. Amer. Ceram. Soc.* **63** (1980) 664.
8. H. SCHMALZRIED, "Solid State Reactions" (Academic, New York and London, 1974) p. 214.
9. B. J. WUENSCH, *Mater. Sci. Res.* **9** (1977) 211.
10. K. M. OSTYN, C. B. CARTER, M. KOEHNE, H. FALKE and H. SCHMALZRIED, *J. Amer. Ceram. Soc.* **67** (1984) 679.
11. R. E. LIESEGANG, *Photo. Archiv.* **21** (1896) 221.
12. D. L. RICOULT and H. SCHMALZRIED, *Ber. Bunsenges. Phys. Chem.* **90** (1986) 135.
13. J. BRYNESTAD and H. FLOOD, *Z. Elektrochem.* **62** (1958) 953.
14. G. W. GROVES and M. E. FINE, *J. Appl. Phys.* **35** (1964) 3587.
15. F. R. N. NABARRO, *Proc. Roy. Soc.* **A175** (1940) 519.
16. C. H. CHEN, M. R. NOTIS and D. B. WILLIAMS, *J. Amer. Ceram. Soc.* **66** (1983) 566.
17. M. SCHNEHAGE, R. DIECKMANN and H. SCHMALZRIED, *Ber. Bunsenges. Phys. Chem.* **86** (1982) 1061.
18. G. J. YUREK and H. SCHMALZRIED, *ibid.* **79** (1975) 255.
19. J. B. HOLT and R. H. CONDIT, *Mater. Sci. Res.* **3** (1966) 25.
20. A. ATKINSON, *Sol. State Ionics* **12** (1984) 309.

Received 20 August  
and accepted 9 October 1986